Image resolution of surface-plasmon-mediated near-field focusing with planar metal films in three dimensions using finite-linewidth dipole sources

Pieter G. Kik,* Stefan A. Maier, and Harry A. Atwater

California Institute of Technology, Thomas J. Watson Laboratory of Applied Physics, Pasadena, California 91125, USA

We study the role of surface plasmons in the near-field focusing of a finite-linewidth point dipole by a planar silver film using three-dimensional finite element calculations. We find that the intensity distribution in the image plane at a distance of 60 nm from the source is narrowed by a factor of 1.4 in the presence of a 30-nm-thick silver film. The lateral field components are found to be focused significantly better. We show that the difference is caused by unavoidable stray fields normal to the lens surface due to the interface charge distribution induced by the presence of surface plasmons.

Recently there has been a surge in theoretical and experimental studies of materials that have simultaneously negative dielectric permittivity ε and magnetic permeability μ, also known as left-handed media (LHM). These materials can be described as having a negative refractive index, as was pointed out by Veselago as early as 1968.[1] Left-handed materials exhibit counterintuitive behavior, such as an inverse Doppler shift, backward Cherenkov radiation, and negative refraction at the interface between a conventional dielectric medium and a LHM. Although there are no known naturally occurring materials with these properties, it is possible to construct a composite material consisting of discrete inductive and resistive elements[2] that effectively behaves as a LHM at microwave frequencies, as long as the building blocks are much smaller than the wavelength λ. Using this approach, Shelby *et al.* were able to experimentally demonstrate negative refraction in a LHM at microwave frequencies.[3] Their findings led to a heated debate on the reality of negative refraction, the apparent violation of causality, and the validity of the dispersion relations used in describing the material properties.[4,5] However, two recent studies unambiguously show negative refraction of a finite Gaussian beam at the interface between a normal dielectric and a LHM by using finite-difference time domain simulations of realistic material systems, and it is shown convincingly that causality is in fact not violated.[6,7]

In his original publication, Veselago showed that negative refraction allows for the construction of a planar lens consisting of a slab of left-handed material with a refractive index opposite to that of its dielectric environment. This type of lens would have several special features setting it apart from conventional lenses. (a) No reflection would occur at the lens surface due to perfect impedance matching with its surroundings. (b) The distance between the object and the image generated by the lens would be fixed, being twice the physical thickness d of the lens. (c) A planar negative index lens has no intrinsic optical axis: the image is always produced opposite the source. The absence of a unique optical axis also implies that these planar lenses cannot be used for magnification. Recently, Pendry[8] pointed out a special feature of negative index lenses that was not discussed by Veselago. Using a mathematical analysis he showed that a negative index lens can in principle generate images with a

resolution better than the diffraction limit. His calculations showed that not only does a slab of a LHM focus propagating electromagnetic (EM) fields, but EM fields that are localized near the source appear to be amplified inside the LHM, resulting in a (partial) recovery of the localized fields in the image plane.

It would be extremely interesting to apply the concept of subdiffraction limit focusing in the visible frequency regime. If successful, such high-resolution imaging could have significant impact in applications such as near-field scanning optical microscopy, high-resolution optical near-field lithography, and optical data storage. However, constructing an artificial negative index material that operates at visible frequencies and that is effectively homogeneous on a wavelength scale poses serious fabrication challenges[9,10] and introduces problems related to surface scattering when the structure sizes approach the electron scattering length in the material used. In his original article Pendry argued that for thin films ($d \ll \lambda$) focusing of electric field components parallel to the lens can occur even in the absence of a negative μ, as long as ε is negative. This is an important claim, since several metals exhibit a negative dielectric constant at optical frequencies, allowing for this type of effect to be achieved in real material systems. For near-field focusing to occur, the dielectric constant of the lens needs to be opposite to that of the surrounding material. This is also the requirement for the existence of localized surface plasmons.[11] Consequently, it has been suggested by several authors that surface plasmons play an important role in the formation of the near-field images. In order to interpret experiments probing subwavelength image formation using fluorescent sources with a finite spatial extent and a finite emission linewidth, a time-dependent three-dimensional analysis is required. However, thus far studies of near-field imaging with planar metal films have all focused on systems in steady state, and involved calculations that were effectively two dimensional,[8,12] were based on dispersionless materials,[13] or both.[14–18]

In this article we study the role of surface plasmons in the near-field imaging of a finite-linewidth point dipole by performing three-dimensional (3D) simulations based on the finite integration technique[19] (FIT) using an accurate description of material dispersion. Our results show that a local oscillating dipole source near a negative ε material can ex-
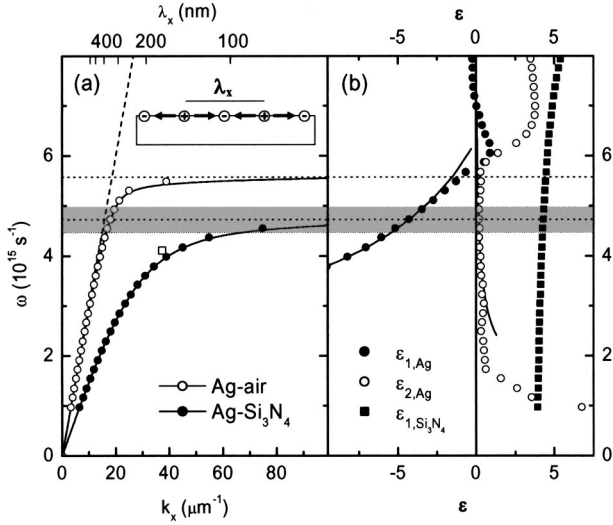
69 045418-1

FIG. 1. (a) Surface plasmon dispersion relation of a silver-air interface and a silver-Si$_3$N$_4$ interface. The solid lines are guides to the eye. The dashed line represents the dispersion of light in air. The shaded area indicates the bandwidth of our excitation pulse. The inset shows a sketch of a surface plasmon charge distribution. (b) Dielectric functions of Si$_3$N$_4$ and Ag.

cite a coherent superposition of surface plasmon oscillations that together produce a sharpened distribution of the *lateral electric field components* in the image plane. We will demonstrate that, due to the charge distribution associated with surface plasmons present at the interface, the *intensity distribution* in the image plane shows less pronounced focusing. Implications of our findings for experiments aimed at demonstrating this effect will be discussed.

To understand the relevance of surface plasmons for near-field imaging, we first need to consider the surface plasmon (SP) dispersion relation of a flat metal surface. Surface plasmons are longitudinal charge density fluctuations that occur at the boundary between a metal and a dielectric (see the inset of Fig. 1). The variations in charge density along the surface are described by a wave vector $k_x = 2\pi/\lambda_x$ with λ_x the surface plasmon wavelength. The SP dispersion relation is given by[11]

$$k_x(\omega) = \frac{\omega}{c} \sqrt{\frac{\varepsilon_m(\omega)\varepsilon_d(\omega)}{\varepsilon_m(\omega) + \varepsilon_d(\omega)}}, \qquad (1)$$

with ω the angular frequency of the plasmon oscillation, c the speed of light in vacuum, and ε_m and ε_d the real parts of the dielectric functions of the metal and the surrounding medium, respectively. The EM fields associated with surface plasmons drop off exponentially normal to the surface. Figure 1(a) shows the dispersion relation of SPs on a silver (Ag) surface in air and in silicon nitride (Si$_3$N$_4$), respectively, calculated using Eq. (1) and the literature values for the dielectric functions of silver[20] and silicon nitride[21] displayed in Fig. 1(b) (circles and squares, respectively). The dielectric constant of air was taken to be 1. The dashed line represents the dispersion relation of light in vacuum, called the light line, given by $\omega = ck_x$. For small values of k_x the SP disper-

sion relation in air lies close to the light line, but as k_x increases the dispersion relation asymptotically approaches $\omega = 5.57 \times 10^{15}$ rad/s (indicated by the top dotted line) corresponding to a free-space wavelength of $\lambda_f = 338$ nm. As can be seen in Fig. 1(b), this corresponds to the condition $\varepsilon_{1,Ag} = -\varepsilon_{air}$. At this frequency, called the surface plasmon frequency ω_{SP}, the slope of the dispersion relation and thus the group velocity v_g approach zero, and the surface supports localized surface plasmons. For a Ag surface in Si$_3$N$_4$ the surface plasmon frequency is found to be 4.73×10^{15} rad/s corresponding to a free-space wavelength of $\lambda_f = 399$ nm. Figure 1 shows the necessary ingredients of near-field imaging: at ω_{SP} surface plasmons can provide charge distributions (and corresponding electric field distributions) with a wide range of high spatial frequencies, all oscillating at the same ω_{SP}. By exciting a coherent superposition of SP oscillations with different wave vectors on a metal surface, it is thus theoretically possible to generate an electric field distribution with a resolution far in excess of the diffraction limit.

We investigate focusing of a point dipole by a 30 nm Ag film supported on a 30 nm free-standing film of Si$_3$N$_4$. We choose this example because it represents a situation that can be achieved experimentally by depositing silver onto silicon nitride membranes. Simulations are performed using a well established FIT based time domain code.[22] The simulation volume spans (500 nm)^3 and contains 2×10^6 grid points. The grid was graded along the z axis (normal to the film surface) resulting in a minimum cell size of (3 nm)^3 at the film location. The source is represented by an oscillating x-polarized dipole (parallel to the surface) that is placed 3 nm away from the silicon nitride surface. In this geometry, the parallel electric field components of the dipole are predicted to be imaged near the silver-air interface. We study two cases, one in which the time-dependent dipole strength is given by a Gaussian-modulated sine wave with a center frequency of 4.73×10^{15} rad/s ($\lambda_f = 399$ nm), corresponding to ω_{SP} of the Ag-Si$_3$N$_4$ interface, and one with $\omega = 4.12 \times 10^{15}$ rad/s ($\lambda_f = 458$ nm), which is significantly removed from ω_{SP}. The pulse bandwidth measured at full width at half maximum (FWHM) was chosen to be 10% of the center frequency. The bandwidth for the high-frequency excitation is indicated by the shaded area in Fig. 1. Note that, because of the finite bandwidth of our excitation pulse, it is important to accurately model the dielectric function of all materials over an extended frequency range. The FIT code used implements a modified Drude model to describe the complex dielectric function of dispersive materials, given by

$$\varepsilon(\omega) = \varepsilon_h - \frac{(\varepsilon_s - \varepsilon_h)\omega_p^2}{(\omega^2 - i\omega\gamma)}, \qquad (2)$$

with ε_h the high-frequency limit of $\varepsilon(\omega)$, ε_s the static dielectric constant, and γ the electron collision frequency in the material. The solid lines in Fig. 1(b) represent the frequency-dependent real ($\varepsilon_{1,Ag}$) and imaginary ($\varepsilon_{2,Ag}$) parts of the silver dielectric function as obtained from Eq. (2) using $\omega_p = 1.72 \times 10^{16}$ rad/s, $\varepsilon_h = 5.45$, $\varepsilon_s = 6.18$, and $\gamma = 8.35 \times 10^{13}$ Hz. These values result in good correspondence with the literature values in the frequency range of interest. The
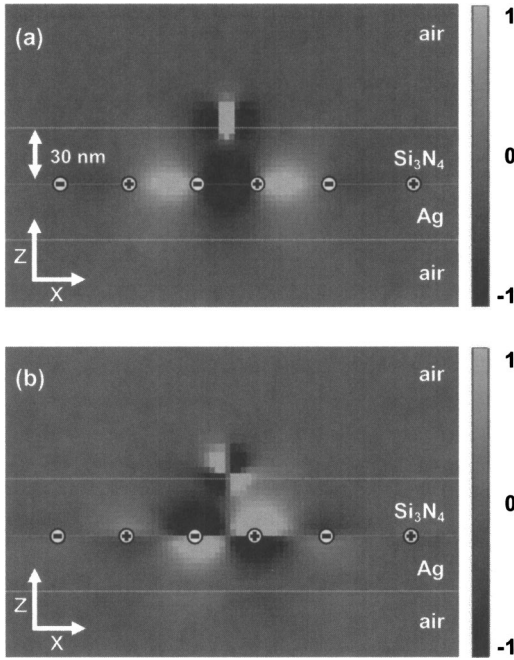
FIG. 2. Snapshots of the electric field distribution near a planar metal film excited with an oscillating dipole at $\omega = 4.73 \times 10^{15}$ rad/s ($\lambda_f = 399$ nm) corresponding to the surface plasmon frequency, showing (a) the lateral component of the electric field (E_x) and (b) the normal component of the electric field (E_z) at $t \approx 25$ fs. The surface plasmon field distribution that is observed at the interface allows for near-field imaging.

number of time steps per optical cycle was 300, and the simulation was run for over 20 optical cycles, allowing the dipole to reach its maximum amplitude. Reducing the bandwidth by a factor of 2, increasing the simulation time by a factor of 2, reducing the time step by a factor of 2, and increasing the number of grid points by a factor of 5 did not significantly alter the simulation results.

Figure 2(a) shows a representative snapshot of the x component of the electric field E_x in the XZ plane near the end of the simulation ($t \approx 25$ fs) for an excitation frequency of 4.73×10^{15} rad/s. This time corresponds to the maximum amplitude of the excitation signal. The color scale is linear, with dark corresponding to negative values of E_x and light corresponding to positive values. The x-polarized dipole is nearing zero magnitude, and at the same time a localized spatially varying electric field distribution is observed at the Ag-Si$_3$N$_4$ interface. This electric field distribution is indicative of an oscillating charge density distribution due to the presence of surface plasmons at the interface. The location of the corresponding charge density maxima and minima is indicated by the $+$ and $-$ signs, respectively. Note that the charge distribution is not perfectly periodic, showing that surface plasmons with different values of k_x are simultaneously present. This can be understood from the dispersion relation shown in Fig. 1: our excitation source is localized in space and contains high-spatial-frequency components, all of which are oscillating within the excitation bandwidth of $\omega_{SP} \pm 10\%$. At these frequencies there exist many allowed SP modes with different values for k_x at the interface. These
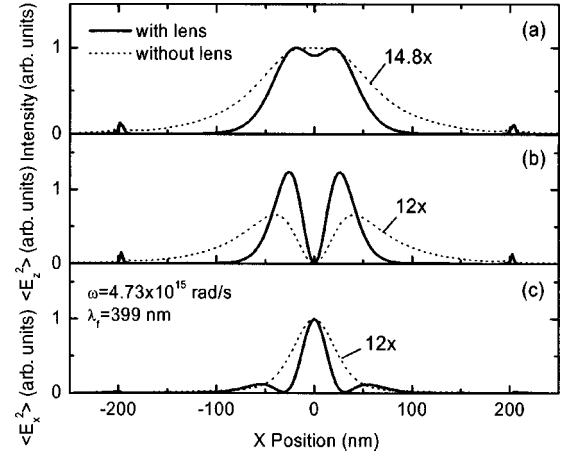

FIG. 3. Time-averaged intensity and field distributions in the image plane of the lens structure shown in Fig. 2 for an excitation frequency of $\omega = 4.73 \times 10^{15}$ rad/s corresponding to ω_{SP}, either with or without a planar silver layer in place.

modes can be resonantly excited by the corresponding spatial frequency components of our point source. The coherent oscillation of the different SP modes leads to the formation of a narrow spatial distribution of E_x in the image plane near the surface of the Ag layer. Note that the electric field distribution is approximately symmetric around the interface, an indication that at this frequency the values for ε are indeed opposite on either side of the interface.[11] Finally, note that the SP field strength in air is small on either side of the film stack, and consequently the surface plasmon dispersion relation is expected to be only weakly perturbed by the finite thickness of the films at these frequencies. Figure 2(b) shows the corresponding distribution of the z component of the electric field (E_z). As expected, E_z peaks near maxima and minima of the charge distribution. Note that E_z and E_x are of comparable magnitude.

Figure 3(a) shows the normalized local intensity I in the image plane along the x direction at a distance of 3 nm (equal to one grid spacing) from the Ag surface, obtained by time averaging the energy density over one optical cycle near the end of the simulation. The solid line represents the configuration depicted in Fig. 2. The dotted line indicates a reference simulation in which the Ag-Si$_3$N$_4$ bilayer has been replaced by a 60-nm-thick film of silicon nitride. The features around $x = -200$ and 200 nm are artifacts due to the finite lateral size of our lens structure. We see that the presence of the silver layer improves the resolution, reducing the FWHM of the intensity distribution in the image plane by a factor of 1.4 from 130 to 93 nm. The intensity distribution in the y direction was found to be reduced from 120 to 50 nm (data not shown). Since the image plane is in the near field of the source dipole, it is no surprise that both these intensity distributions have a width that is less than the diffraction limit.

The intensity distributions displayed in Fig. 3(a) contain contributions from both E_x and E_z. In Figs. 3(b) and 3(c) we plot the corresponding time-averaged values for E_z^2 and E_x^2, indicated as $\langle E_z^2 \rangle$ and $\langle E_x^2 \rangle$, respectively. The values for $\langle E_x^2 \rangle$ in Fig. 3(c) were normalized to 1, and the values for $\langle E_z^2 \rangle$
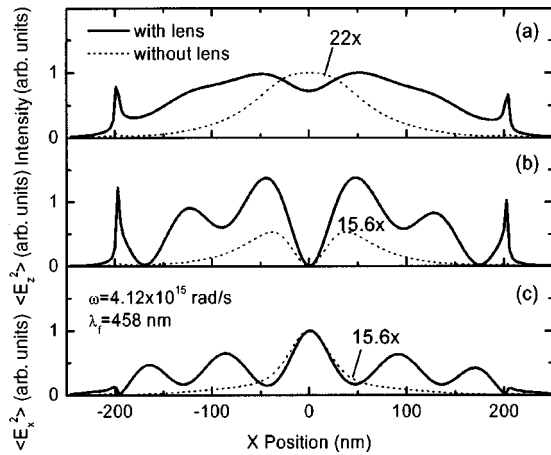
FIG. 4. Time-averaged intensity and field distributions in the image plane of the lens structure shown in Fig. 2 for an excitation frequency of $\omega = 4.12 \times 10^{15}$ rad/s, below ω_{SP}, either with or without a planar silver layer in place.

were scaled by the same factor, allowing for direct comparison of their magnitudes. Several points should be noted. First, the $\langle E_x^2 \rangle$ distribution is much sharper than the intensity distribution in Fig. 3(a). Second, the width of the $\langle E_x^2 \rangle$ distribution is reduced by a factor of ~ 2 from 51 to 27 nm. Finally, the $\langle E_z^2 \rangle$ distribution shows two pronounced peaks on either side of $x = 0$.

The features observed in Fig. 3 can be understood by keeping in mind that the generation of the localized image requires a localized lateral electric field distribution. This is provided by surface plasmons that generate localized charge maxima at the interface to the left and to the right of the image [see Fig. 2(a)], resulting in a localized lateral electric field at the image position. However, the same charges that provide the lateral electric field also generate a significant normal field [see Fig. 2(b)] on either side of the image, broadening the intensity distribution in the image plane. This normal field distribution is an unavoidable by-product of the charge distribution required to achieve near-field imaging with planar metal films. Note that these results imply that in applications involving the use of near-field *intensity*, such as near-field lithography, the maximum resolution enhancement will be less than is possible for the lateral field components.

To illustrate the importance of excitation at ω_{SP}, in Fig. 4 we show I, $\langle E_z^2 \rangle$, and $\langle E_x^2 \rangle$ as obtained for the case of $\omega = 4.12 \times 10^{15}$ rad/s corresponding to $\lambda_f = 458$ nm. At this frequency, the intensity distribution in Fig. 4(a) is in fact *broadened* by the presence of the silver film. This can be understood as follows: at frequencies below ω_{SP} each frequency relates to a SP mode with one specific k_x with a finite group velocity (see Fig. 1). Consequently, locally exciting the interface below ω_{SP} results in the resonant excitation of counterpropagating SP modes with identical $|k_x|$, causing the sinusoidal intensity distribution observed in Fig. 4(c). The $\langle E_x^2 \rangle$ distribution in Fig. 4(c) has a spatial period of ~ 85 nm, corresponding to a surface plasmon wavelength of ~ 170 nm, or $k_x \approx 37 \ \mu\text{m}^{-1}$. This value, indicated by the open square in Fig. 1, indeed lies close to the calculated SP dispersion relation.
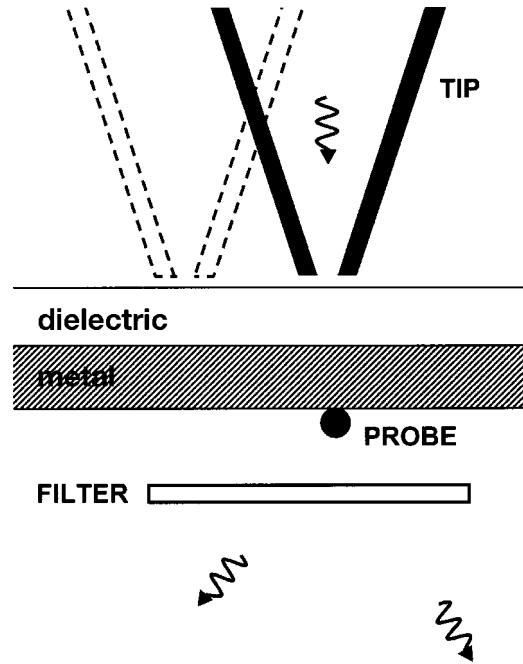

FIG. 5. Sketch of a possible experimental configuration that can be used to demonstrate near-field focusing using planar metal films. Shown are the tip of a near-field optical microscope, the imaging structure, and a local probe.

These results have important consequences for experiments aiming to demonstrate near-field focusing with planar metal films. To explain this in more detail we will consider three different experimental conditions based on the configuration shown in Fig. 5. In all cases, the source dipole is represented by the tip of a near-field scanning optical microscope, which is illuminating the metal-dielectric bilayer at the frequency corresponding to the optimum imaging condition (ω_{SP}). The tip is raster scanned over the sample surface. A nanoscale optical probe is placed in the image plane. We consider three different types of local probe. (a) A *dye-doped particle*, containing fluorophores absorbing at ω_{SP} and emitting at a longer wavelength. The redshifted intensity can be detected independently by filtering out the illumination wavelength with a bandpass filter (labeled "filter" in Fig. 5). Fluorescence will be detected whenever the tip image overlaps with the probe particle, allowing for a measurement of the image resolution in the image plane. Note that the detected emission intensity will be proportional to the near-field *intensity* at the particle position, corresponding to the image distribution shown in Fig. 3(a). Similarly, if one tries to write nanoscopic features in a photoresist layer using the tip image as a local illumination source, the resolution will again be determined by the near-field intensity distribution in Fig. 3(a) and not by the more sharply focused lateral field components shown in Fig. 3(b). (b) An *anisotropic molecule*, again emitting at a redshifted wavelength. An absorption cross section that depends on the orientation of the electric field allows for selective sampling of individual field components. Depending on the orientation of the molecule (in plane or out of plane), this would result in an image resolution corresponding to that displayed in either Fig. 3(b) or

3(c). (c) A *strong scatterer*, e.g., a metallic nanoparticle. In this case the illumination signal cannot be filtered out since illumination and scattering occur at the same frequency. The total signal detected in the far field will thus be a coherent superposition of radiating components from the source and the scattered intensity from the nanoparticle. Note that the far-field intensity detected normal to the film surface will nevertheless be a measure of the lateral near-field components, since normal field components do not radiate in this direction. This special case will be discussed in greater detail in a forthcoming article.

To summarize, we have performed 3D finite-difference simulations of near-field focusing of a finite-linewidth oscillating point dipole by a 30-nm-thick planar silver film on a 30-nm-thick silicon nitride film. The silver film reduces the width of the lateral field components $\langle E_x^2 \rangle$ in the image plane by a factor of 2 for a dipole excitation at the surface plasmon frequency of the Ag-Si$_3$N$_4$ interface. The narrowing is caused by the resonant excitation of a coherent superposition of surface plasmon modes with different wave vectors k_x at the silver–silicon nitride interface. Under identical conditions, the width of the *intensity* distribution in the image plane is reduced by a factor of 1.4. The difference is caused by the presence of the electric fields normal to the interface associated with the surface-plasmon-induced charge distribution at the interface. The presence of these normal fields is an inherent property of near-field imaging by planar metal films and cannot be ignored in most practical situations. Finally, we show that excitation at a frequency below the surface plasmon resonance frequency results in the resonant excitation of propagating surface plasmons, producing electric field and intensity distributions in the image plane that have a *reduced* resolution compared to those in the absence of a lens.

---

*Present address: University of Central Florida, School of Optics/ CREOL/FPCE, Orlando, Florida 32816, USA; Electronic address: kik@creol.ucf.edu

[1] V. G. Veselago, Sov. Phys. Usp. **10**, 509 (1968).

[2] J. B. Pendry, A. J. Holden, D. J. Robbins, and W. J. Stewart, IEEE Trans. Microwave Theory Tech. **47**, 2075 (1999).

[3] R. A. Shelby, D. R. Smith, and S. Schultz, Science **292**, 77 (2001).

[4] P. M. Valanju, R. M. Walser, and A. P. Valanju, Phys. Rev. Lett. **88**, 187401 (2002).

[5] N. Garcia and M. Nieto-Vesperinas, Phys. Rev. Lett. **88**, 207403 (2002).

[6] D. R. Smith, D. Schurig, and J. B. Pendry, Appl. Phys. Lett. **81**, 2713 (2002).

[7] S. A. Cummer, Appl. Phys. Lett. **82**, 2008 (2003).

[8] J. B. Pendry, Phys. Rev. Lett. **85**, 3966 (2000).

[9] C. Shvetz, Phys. Rev. B **67**, 035109 (2003).

[10] V. A. Podolskiy, A. K. Sarychev, and V. M. Shalaev, Opt. Express **11**, 735 (2003).

[11] H. Raether, *Surface Plasmons* (Springer-Verlag, Berlin, 1988).

[12] J. T. Shen, and P. M. Platzman, Appl. Phys. Lett. **80**, 3286 (2002).

[13] N. Fang, Z. Liu, T-J. Yen, and X. Zhang, Opt. Express **11**, 682 (2003).

[14] E. Shamonina, V. A. Kalinin, K. H. Ringhofer, and L. Solymar, Electron. Lett. **37**, 1243 (2001).

[15] N. Fang and X. Zhang, Appl. Phys. Lett. **82**, 161 (2003).

[16] G. Gómez-Santos, Phys. Rev. Lett. **90**, 077401 (2003).

[17] D. R. Smith, D. Schurig, M. Rosenbluth, S. Schultz, S. A. Ramakrishna, and J. B. Pendry, Appl. Phys. Lett. **82**, 1506 (2003).

[18] P. Kolinko and D. R. Smith, Opt. Express **11**, 640 (2003).

[19] S. Gutschling, H. Kruger, and T. Weiland, Int. J. Numer. Model. **13**, 329 (2000).

[20] P. B. Johnson and R. W. Christy, Phys. Rev. B **6**, 4370 (1972).

[21] E. D. Palik, *Handbook of Optical Constants* (Academic, London, 1985).

[22] Computer code MAFIA, Computer Simulation Technology, Darmstadt, Germany.